

ARTICLE

Slow-Onset Inhibition of the FabI Enoyl Reductase from *Francisella tularensis*: Residence Time and *in Vivo* Activity

Hao Lu[†], Kathleen England[‡], Christopher am Ende[†], James J. Truglio[§], Sylvia Luckner[¶], B. Gopal Reddy[†], Nicole L. Marlenee[‡], Susan E. Knudson[‡], Dennis L. Knudson[‡], Richard A. Bowen^{‡,*}, Caroline Kisker[¶], Richard A. Slayden[‡], and Peter J. Tonge^{†,*}

[†]Institute for Chemical Biology & Drug Discovery, Department of Chemistry, Stony Brook University, Stony Brook, New York 11794-3400, [‡]Rocky Mountain Regional Center of Excellence and Department of Microbiology, Immunology and Pathology, Colorado State University, Fort Collins, Colorado 80523-1682, [§]Center for Structural Biology, Stony Brook University, Stony Brook, New York 11794-5115, and [¶]Rudolf Virchow Center for Experimental Biomedicine, Institute for Structural Biology, University of Würzburg, Versbacher Str. 9, 97078 Würzburg, Germany

F*Francisella tularensis* is a highly virulent and contagious Gram-negative intracellular bacterium that causes the disease tularemia in mammals (1). The ability of *F. tularensis* to be aerosolized, coupled with the small number of bacteria required to cause disease and the ability of the bacterium to survive for weeks in a cool, moist environment, have raised the possibility that this organism could be used deliberately as an infectious agent (2). Consequently, NIAID has classified *F. tularensis* as a Category A priority pathogen. Streptomycin and gentamicin are currently used as chemotherapeutics to treat tularemia; however, neither of them can be orally administered. In addition, despite the availability of drugs such as the aminoglycosides, macrolides, chloramphenicol, and fluoroquinolones, infection can result in a mortality as high as 40%. Taken together, there is a pressing need to develop chemotherapeutics with novel mechanisms of action for the treatment of tularemia.

The fatty acid synthesis pathway in *F. tularensis* is a type II (FAS II) dissociated synthase where individual reactions are carried out by separate proteins. Importantly, eukaryotes utilize the type I fatty acid biosynthesis multienzyme complex (FAS I), which is fundamentally different from the FAS II pathway in which each activity is encoded by a separate polypeptide (3). The NADH-dependent enoyl reductase (FabI), which catalyzes the last reaction in the elongation cycle, is known to be an essential component in the FAS-II system (4). Genetic knockout and knockdown experiments together

ABSTRACT *Francisella tularensis* is a highly virulent and contagious Gram-negative intracellular bacterium that causes the disease tularemia in mammals. The high infectivity and the ability of the bacterium to survive for weeks in a cool, moist environment have raised the possibility that this organism could be exploited deliberately as a potential biological weapon. Fatty acid biosynthesis (FAS-II) is essential for bacterial viability and has been validated as a target for the discovery of novel antibacterials. The FAS-II enoyl reductase *ftuFabI* has been cloned and expressed, and a series of diphenyl ethers have been identified that are subnanomolar inhibitors of the enzyme with MIC₉₀ values as low as 0.00018 $\mu\text{g mL}^{-1}$. The existence of a linear correlation between the K_i and MIC values strongly suggests that the antibacterial activity of the diphenyl ethers results from direct inhibition of *ftuFabI* within the cell. The compounds are slow-onset inhibitors of *ftuFabI*, and the residence time of the inhibitors on the enzyme correlates with their *in vivo* activity in a mouse model of tularemia infection. Significantly, the rate of breakdown of the enzyme-inhibitor complex is a better predictor of *in vivo* activity than the overall thermodynamic stability of the complex, a concept that has important implications for the discovery of novel chemotherapeutics that normally rely on equilibrium measurements of potency.

*Corresponding authors,
richard.slayden@colostate.edu,
peter.tonge@sunysb.edu.

Received for review June 3, 2008
and accepted February 1, 2009.
Published online February 10, 2009
10.1021/cb800306y CCC: \$40.75
© 2009 American Chemical Society

with studies utilizing small molecule FabI inhibitors have demonstrated that FabI is essential for bacterial cell growth, thus making it an attractive target for drug discovery (5–8). Several classes of chemicals have been identified that are picomolar inhibitors of FabI (9–12), including the diphenyl ether triclosan, a broad spectrum chemotherapeutic with activity against a variety of important pathogens including *E. coli*, methicillin-resistant *S. aureus*, and *M. tuberculosis* (13–18).

In this study, we expressed and purified the FabI from *F. tularensis* (ftuFabI) and identified a series of diphenyl ether-based ftuFabI enzyme inhibitors. The most potent alkyl diphenyl ether is a slow-onset inhibitor with a K_i value of 0.44 nM and MIC_{90} value of 0.00018 $\mu\text{g mL}^{-1}$. The existence of a linear correlation between K_i and MIC_{90} values supports the conclusion that the compounds target ftuFabI within the cell. A selection of the ftuFabI inhibitors are active in a mouse model of *F. tularensis* infection; however, the increase in mean time to death and percent survival caused by these compounds correlates best with the residence time of the inhibitor on the enzyme (19, 20) rather than the overall thermodynamic stability of the enzyme–inhibitor complex (K_i). This observation has important implications for rational drug design, which is often driven solely by equilibrium measurements of inhibitor action, such as the determination of K_i or IC_{50} values, rather than by considerations of parameters such as the residence time of the drug on the target.

RESULTS AND DISCUSSION

Steady-State Kinetic Analysis of ftuFabI Inhibition by Triclosan. The equilibrium dissociation constant of triclosan (**1**) (Figure 1) from ftuFabI was determined by preincubating ftuFabI and triclosan in the presence of a high concentration of NADH and a low concentration of NAD^+ (compared to their K_d values) (21). Apparent inhibition constants (K_i') were measured at six different NAD^+ concentrations (10, 15, 20, 50, 100, and 200 μM) in the presence of 250 μM NADH, and the data were fit to eqs 2–4 with $K_{m,\text{NAD}}$ constrained to 21 mM, which was calculated from eq 5 using $K_{m,\text{NADH}} = 18.8 \mu\text{M}$. Equation 2 gave the best fit to the data, demonstrating that triclosan is an uncompetitive inhibitor with respect to NAD^+ with a value of $51 \pm 3 \text{ pM}$ at saturating NAD^+ . To estimate the affinity of triclosan for the E-NADH complex, the data were reanalyzed using equation 4 to provide a K_i value of $53 \pm 1 \text{ pM}$ and a poorly determined

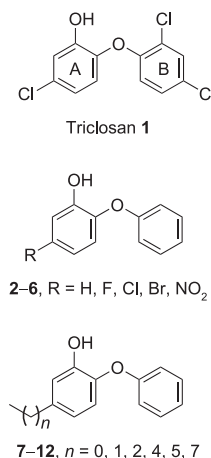
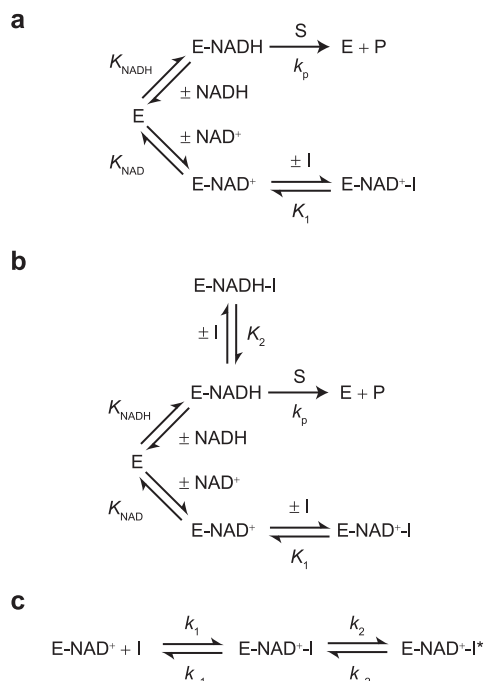


Figure 1. Structure of triclosan and the diphenyl ether ftuFabI inhibitors.

value for K_2 of $5 \pm 35 \mu\text{M}$, indicating that triclosan binds approximately 90,000-fold more tightly to E-NAD⁺ than to E-NADH (Scheme 1, panel a).

Structure–Reactivity Analysis of ftuFabI Inhibition by Triclosan and Diphenyl Ethers. Evidence from X-ray structural (17, 22–24) and kinetic studies (21, 25) indicate that triclosan forms a very stable ternary complex with the FabI enzyme from *E. coli* (ecFabI), which is stabilized by a π – π stacking interaction between the hydroxychlorophenyl ring (ring A, Figure 1) and the nicotinamide ring of the NAD⁺ cofactor, together with an edge-on π interaction between the 5-chloro group and the aromatic ring of F203 (Figure 2, panel a). Structural studies have previously shown that the major conformational change that occurs upon binding of triclosan to ecFabI-NAD⁺ is the ordering of the “substrate-binding” loop (Figure 2, panel b). This loop (residues 195–200) is disordered in the binary complex (Figure 2, panel b) but adopts an α -helical conformation to cover the active site of the enzyme when triclosan is bound (17, 22, 26, 27). We have previously postulated that the slow-onset inhibition of ecFabI by triclosan is coupled to the ordering of this loop (26). The high similarity between the structure of the ecFabI-NAD⁺ complex and the 2.9 Å resolution structure of the binary ftuFabI-NAD⁺ complex reported here (Figure 2, panel c), provide a firm foundation for extending the conclusions on the ecFabI system to ftuFabI. Similar to ecFabI, the substrate binding loop in the ftuFabI-NAD⁺ complex is also disordered,

SCHEME 1. Kinetic schemes for the interaction of ftuFabl with inhibitors^a



^a a) Inhibitor binds exclusively to the E-NAD⁺ form of the enzyme with an equilibrium dissociation constant of K_{Ii} . b) Inhibitor binds to both E-NAD⁺ and E-NADH forms of the enzyme with equilibrium dissociation constants of K_1 and K_2 , respectively. c) Slow-onset inhibition of ftuFabl in which formation of the final E-I* inhibitor complex occurs in two steps, the second of which is the slow step.

and we postulate that slow-onset inhibition of ftuFabl is also coupled to loop ordering.

To probe the role of specific interactions in the ternary ftuFabl complex, we synthesized a series of diphenyl ether compounds (Figure 1). In ecFabl it was found that ring B points away from the active site and participates in several unfavorable steric interactions with the enzyme based on the observation that 5-chloro-2-phenoxyphenol (**4**) has a 7-fold higher affinity compared with that of triclosan (25). However, in our studies compound **4** showed a 37-fold decrease in affinity, indicating that the two chlorine atoms on ring B form important interactions with ftuFabl. In addition, for the other slow-onset inhibitors of ftuFabl that lacked chlorine atoms on ring B (**4**, **5**, **7–12**), binding to both

E-NAD⁺ and E-NADH could be observed (Supplementary Figure S1). The dependence of K_i' on $[\text{NAD}^+]$ was fit to eq 4 to obtain the inhibition constants for both forms of the enzyme (Table 1). These data indicate that the primary effect of removing the B ring chlorines is a specific effect on the affinity of the inhibitor for the E-NAD⁺ form of the enzyme. Thus, all slow-onset inhibitors have similar affinities for E-NADH, and structural changes to both A and B rings principally modulate the affinity of the analogues for the E-NAD⁺ product complex. Although the precise structural basis for this effect will require additional structural data, one possibility is that the affinity of each inhibitor for the E-NAD⁺ complex is critically dependent on the precise orientation of the A ring with respect to the oxidized nicotinamide ring and thus the strength of the π -stacking interaction between inhibitor and cofactor.

It has been demonstrated that the electronic and steric properties of ring A play a key role in determining the affinity of the diphenyl ether inhibitors for ecFabl. The importance of the 5-chloro group on ring A for binding to ftuFabl was initially explored by removing the chlorine to generate analogue **2**, which binds 1200-fold less tightly to ftuFabl than does analogue **4**. In addition, analogue **2** was no longer a slow-onset inhibitor, indicating that a substituent on the A ring is essential for triggering loop ordering. To investigate this effect in more detail, we incorporated other halogen atoms into ring A and also replaced the 5-chloro group with alkyl substituents of different lengths (**3**, **5**, **7–12**). All of the alkyl-substituted diphenyl ethers (**7–12**) were shown to be slow, tight-binding inhibitors of ftuFabl. Since the 5-chloro substituent points to a hydrophobic pocket for the fatty acid substrate, it is quite possible that replacement of this substituent with a larger and more hydrophobic group will increase the affinity of the inhibitor for the enzyme. However, the data in Table 1 indicate that analogues with smaller alkyl chains generally bound more tightly to the enzyme, with analogue **9** (5-propyl-2-phenoxyphenol) exhibiting the highest affinity for the enzyme.

A remarkable observation is that replacement of the 5-chloro group with a fluorine results in a compound (5-fluoro-2-phenoxyphenol, **3**) that is not a slow-onset inhibitor and that exhibits a 150-fold decrease in binding affinity compared with those of 5-chloro-2-phenoxyphenol (**4**) and 5-methyl-2-phenoxyphenol (**7**). The $\text{p}K_a$ values of **3** and **4** are almost identical, in agreement with

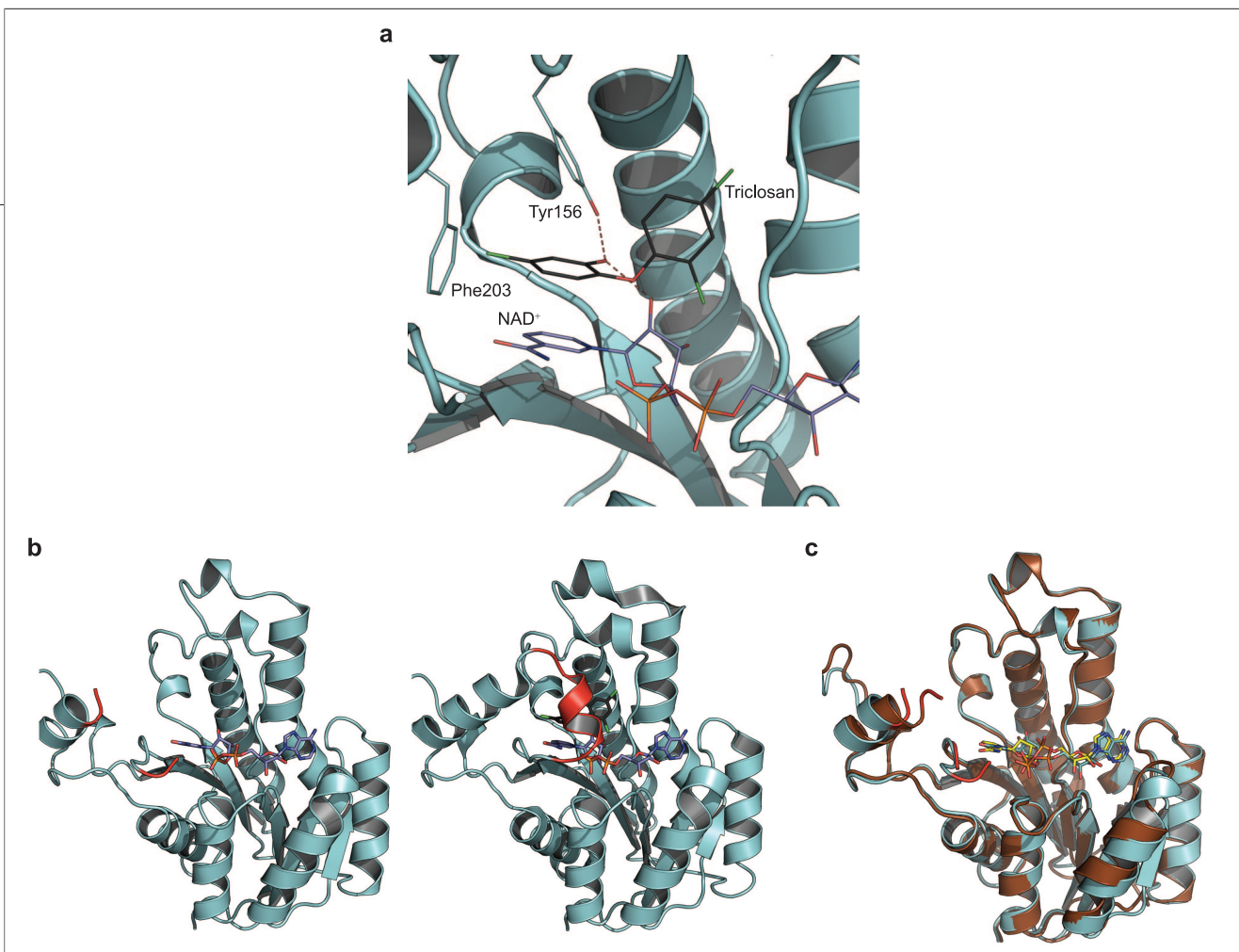


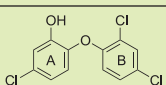
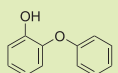
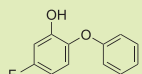
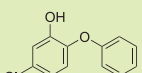
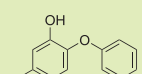
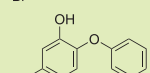
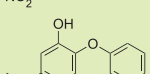
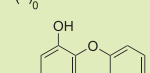
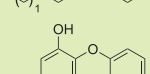
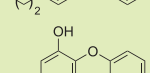
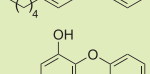
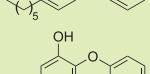
Figure 2. X-ray structures of ecFabI and ftuFabI. **a)** Ribbon presentation of *E. coli* FabI with a close-up view of the active site. The carbon atoms of the triclosan molecule are shown in black and in the NAD⁺ molecule in blue. Oxygen atoms are depicted in red, chloride atoms in green, nitrogen in blue, and phosphorus in orange. **b)** Loop ordering upon triclosan binding. The left panel shows the *E. coli* FabI (pdb code 1dfi) with bound NAD⁺ (blue) with the loop ends marked in red. The right panel shows the ternary triclosan-NAD⁺ *E. coli* FabI structure (pdb code 1qg6) with the loop ordered into a helix (amino acids 194–201 shown in red). **c)** Superposition of *E. coli* FabI with bound NAD⁺, both shown in cyan and *F. tularensis* FabI shown in brown with bound NAD⁺ (yellow). In both structures the active site loop is disordered; the loop ends are marked in red. Superpositions were calculated with Superpose using secondary structure matching (43) implemented in the ccp4 program suite (44). All model illustrations were prepared with PyMOL (45).

electrostatic potential calculations (25), and thus the difference in affinity of **3** and **4** for ftuFabI may arise from the slightly smaller van der Waals radius of fluorine compared with that of chlorine (0.45 Å), which translates to a ~ 9 Å³ reduction in molecular volume of **3** compared with that of **4**. If the loss of slow-onset inhibition is primarily due to the smaller size of the fluorine atom, then replacement of this group with a more bulky substituent might be expected to restore loop ordering, and indeed the bromo (**5**) and methyl (**7**) analogs, which have molecular volumes ~ 5 Å³ larger than that of **4**, as well as the propyl (**9**) and pentyl (**10**) analogs, are all slow-onset inhibitors. These data are in agreement with previous studies on the *E. coli* FabI (25, 28), where it was concluded that the shape of the inhibitor was the principal determinant in modulating the affinity of diphenyl ether inhibitors for the enzyme. Interestingly, however,

incorporation of the larger but more electronegative nitro group (**6**) actually reduced binding affinity 3-fold compared with that of **3** and also resulted in a compound that was no longer a slow-onset inhibitor. Since **6** has a molecular volume that is only slightly larger (~ 3 Å³) than that of **5** or **7**, the reduction in binding affinity of the nitro analog compared to diphenyl ethers bearing, for example, chloro, bromo, or methyl substituents, likely results from a decrease in electron density of the A ring and a weakening of the π – π stacking interaction between this ring and the electron-deficient positively charged nicotinamide ring of NAD⁺.

In summary, the SAR studies reflect the subtle interplay of steric and electronic effects that modulate inhibition in the FabI class of enoyl reductases (25, 28). For ftuFabI, a 5-chloro or 5-bromo substituent is essential for slow, tight-binding inhibition, whereas incorporation

TABLE 1. Enzyme inhibition and *in vitro* antibacterial activity of the ftuFabI inhibitors

Compound	MIC ₉₀ (μg mL ⁻¹)	Inhibition constants and mode of inhibition		
		K _i (nM) ^a	K ₂ (nM) ^b	Type of inhibition
 1	0.000015 ± 0	0.051 ± 0.003	5 ± 35 μM	Slow-onset
 2	2.5 ± 0.2	2260 ± 107 ^c		Rapid equilibrium
 3	0.32 ± 0.02	289 ± 11 ^c		Rapid equilibrium
 4	0.001 ± 0.001	1.9 ± 0.1	308 ± 6	Slow-onset
 5	0.004 ± 0.001	7.1 ± 0.2	149 ± 2	Slow-onset
 6	0.21 ± 0.05	789 ± 13 ^c		Rapid equilibrium
 7	0.16 ± 0.07	1.9 ± 0.1	247 ± 5	Slow-onset
 8	0.03 ± 0.001	2.1 ± 0.1	311 ± 20	Slow-onset
 9	0.00018 ± 0.00014	0.44 ± 0.02	696 ± 70	Slow-onset
 10	0.0012 ± 0.0002	1.3 ± 0.1	525 ± 8	Slow-onset
 11	0.16 ± 0.06	2.7 ± 0.1	331 ± 6	Slow-onset
 12	0.66 ± 0.14	23.6 ± 1.2	192 ± 2	Slow-onset
Gentamicin	4	ND	ND	ND
Streptomycin	2	ND	ND	ND
Doxycycline	0.75 ± 0.35	ND	ND	ND

^aK_i refers to inhibition constant binding to E-NAD⁺. ^bK₂ refers to inhibition constant binding to E-NADH. ^cK_i is actually the K_{iS} value for a rapid, reversible inhibitor. ND, not determined.

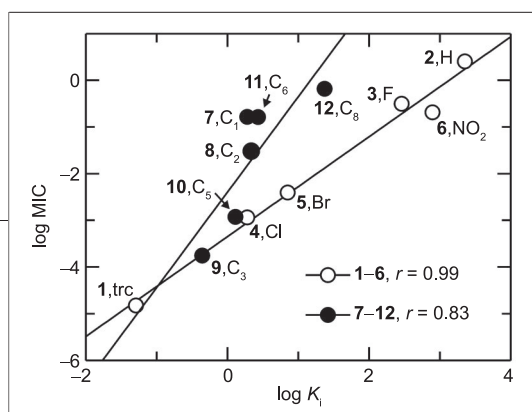


Figure 3. Linear correlation between the log MIC₉₀ and log K₁ values for triclosan and the diphenyl ether inhibitors. Linear fits are shown for two groups of compounds, 1–6 and 7–12.

phobic interactions in the substrate binding pocket. In addition, the π – π stacking interaction between ring A and the NAD⁺ nicotinamide ring is also important for slow-onset enzyme inhibition, as shown by the dramatic impact of introducing a 5-nitro substituent into the inhibitor.

Correlation Between K₁ and MIC Values. Minimum inhibitory concentrations (MIC₉₀) of triclosan and the diphenyl ether inhibitors were obtained against *F. tularensis* LVS. Notably, the diphenyl ethers have more favorable MIC₉₀ values than clinically used drugs (Table 1). Specifically, the best diphenyl ether analog (**9**) is more than 22,000-fold and 4,000-fold more potent than gentamicin and doxycycline, respectively. Significantly, a positive linear correlation between log K₁ and log MIC₉₀ exists for the diphenyl ether derivatives (Figure 3), which strongly suggests that ftuFabI is the primary cellular target for these compounds. Data fitting reveals that the compounds fall into two groups: those

of hydrophobic alkyl chains of up to three carbons increases the affinity of the inhibitor for the enzyme, presumably as a result of favorable hydrophobic interactions in the substrate binding pocket. In contrast, for those compounds for which the residence time of the inhibitor on the enzyme was measured (Table 2), no correlation could be observed between the length of time the inhibitor remained bound to the enzyme and the MIC values.

In Vivo Antibacterial Activity and Residence Time. A rapid animal model of infection was used to evaluate the *in vivo* efficacy of ftuFabI inhibitors against *F. tularensis*. Initially, the *in vitro* cytotoxicity of the selected compounds was determined using a Vero cell assay that suggested that the compounds chosen for analysis had high therapeutic indices with LC₅₀/MIC₉₀ ratios ranging from 600 to 10⁶ (Table 2). In addition, all compounds had maximum tolerated doses of >300 mg kg⁻¹. Animals in the infection model were treated for 5 consecutive days, starting from the day of infection and then monitored for death for an additional 5 days. In general, our experiments showed that all treated animals survived longer than untreated control animals, indicating that diphenyl ethers have antibacterial activity and are able to reduce the bacterial load. In the 10-day animal model of infection, all selected compounds (**1**, **4**, **8**, **9**, and **11**) demonstrated efficacy, with longer median survival values in comparison to untreated control animals whose mean time to death value was 5.2 days

TABLE 2. Rate constants for ftuFabI inhibition as well as *in vitro* and *in vivo* antibacterial activity of selected diphenyl ethers

Inhibitor	k_2 (min ⁻¹)	k_{-2} (min ⁻¹)	Residence time (min) ^a	K_1^{app} (nM)	K_1 (nM) ^b	MIC ₉₀ (μg mL ⁻¹)	Cytotoxicity LC ₅₀ (μg mL ⁻¹) ^c	Median survival ^d	% Survival ^e
Triclosan (1)	0.56 ± 0.04	0.025 ± 0.003	40 ± 3	407 ± 48	0.051 ± 0.003	0.000015 ± 0	14 ± 1	7.8	22
4	0.11 ± 0.01	0.033 ± 0.002	30 ± 2	665 ± 70	1.9 ± 0.1	0.001 ± 0.001	60 ± 14	6.8	11
8	0.13 ± 0.01	0.048 ± 0.001	21 ± 1	1080 ± 110	2.1 ± 0.1	0.03 ± 0.001	65 ± 2	6.1	0
9	1.66 ± 0.01	0.017 ± 0.002	59 ± 2	375 ± 6	0.44 ± 0.02	0.00018 ± 0.00014	62 ± 3	7.8	39
11	0.90 ± 0.01	0.007 ± 0.002	143 ± 14	117 ± 2	2.7 ± 0.1	0.16 ± 0.06	101 ± 2	^f	100
control	na ^g	na	na	na	na	na		5.2	0

^aResidence time = $1/k_{\text{off}}$ where $k_{\text{off}} = k_{-1}k_{-2}/(k_{-1} + k_2 + k_{-2})$. In the two-step slow-onset inhibition mechanism, $k_{-1} \gg k_2$ and k_{-2} , hence $k_{\text{off}} \approx k_{-2}$ (**19**). ^b K_1 is the thermodynamic dissociation constant taken from Table 1. ^cCytotoxicity was determined using Vero cells. Note that the maximum tolerated dose was >300 mg kg⁻¹ for each compound evaluated in the animal model of infection. ^dAll drugs were delivered at 200 mg kg⁻¹ ip once a day for 5 days starting from the day of infection, with observation for an additional 5 days. Animals were sacrificed at day 10. Each study was conducted with 9 animals, and data are means for one (**4** and **8**), two (**1** and **9**), or three (**11**) studies. For one of the studies with **9**, drug was administered ip at 100 mg kg⁻¹. ^ePercent survival is percent of animals that survived to day 10. ^fMedian survival is undefined for **11** because no animals died during the study. ^gna, not applicable.

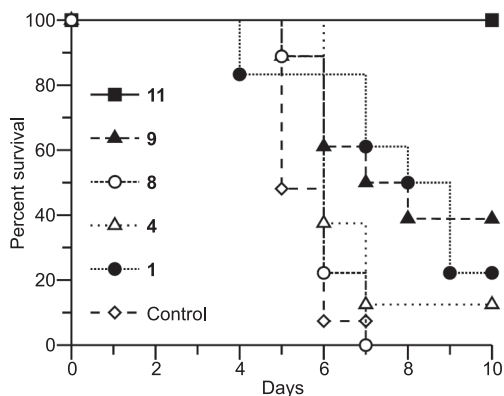


Figure 4. Survival plots for mice infected with *F. tularensis* Schu4 and treated with compounds **1**, **4**, **8**, **9**, and **11**.

(Figure 4 and Table 2). Although all of the other compounds reduced bacterial load and delayed animal death, compound **11** demonstrated greatest efficacy. Importantly, **11** prevented the death of all infected animals to the end of the 10-day study period (100% survival). Consequently, the mean time to death for compound **11** is undefined.

To provide further insight into the *in vivo* activity of the compounds, we used progress curve analysis to evaluate the rate constants for formation and breakdown of the final E-I* complex (29, 30). On the basis of the preincubation experiments, we already knew that the potency of the slow-onset inhibitors increased as the concentration of NAD⁺ increased. Hence NAD⁺

(200 μ M) was added at the beginning of the reaction so that product formation would not affect inhibitor affinity during the reaction. The progress curves showed that the turnover velocity decreased exponentially with time, from an initial velocity, v_i , to a final steady-state velocity, v_s (Figure 5, panel a). Higher concentrations of inhibitor caused the steady state to be reached more quickly and to give lower values of v_s . This behavior demonstrates that the diphenyl ethers are slow-onset reversible inhibitors that interact rapidly with the enzyme to form an initial complex, E-NAD⁺-I and then slowly isomerize to a more stable final inhibited complex, E-NAD⁺-I* (Scheme 1, panel c) (29), which we speculate is the loop ordering step. Consistent with the mechanism shown in Scheme 1, panel c, the k_{obs} values obtained from fitting the data to eq 7 displayed a hyperbolic dependence on the concentration of inhibitor (Figure 5, panel b), while subsequent nonlinear curve fitting using eq 8 gave pre-steady-state constants (k_2 , k_{-2} , and K_1^{app}) for each inhibitor (Table 2). On the basis of the assumption that the rate-limiting step for breakdown of the E-I* complex is isomerization of E-I* to E-I (k_{-2}), k_{-2} can be used to calculate the residence time of the inhibitor on the enzyme. This analysis provided residence times of 40, 30, 21, 59 and 143 min for **1**, **4**, **8**, **9**, and **11**, respectively (Table 2). Interestingly, although triclosan has the highest thermodynamic affinity for ftuFabI and is the most potent compound in the *in vitro* antibacterial assays, compound **11** has the longest residence time on the enzyme. This is significant because

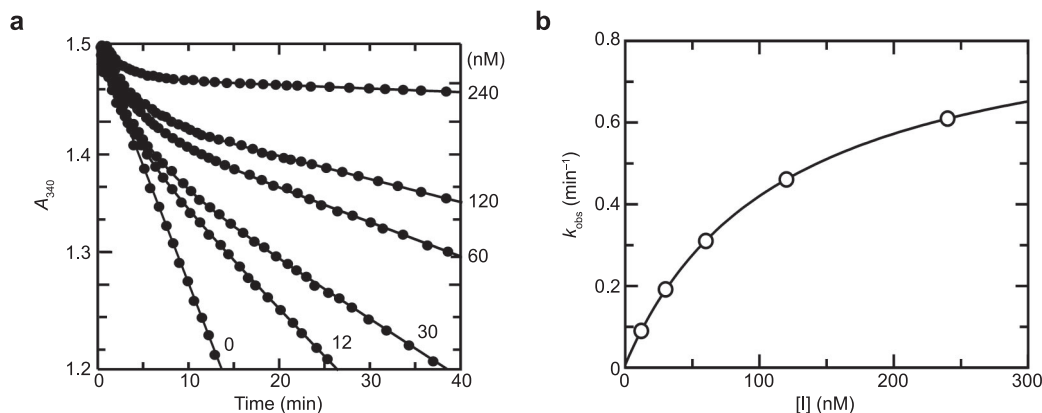


Figure 5. Progress curve analysis of the inhibition of ftuFabI by compound **10**. **a**) Time-dependent inactivation of ftuFabI by compound **11**. The solid curves represent the best fit of the data to eq 7 for slow-onset inhibition. **b**) k_{obs} values from panel a plotted as a hyperbolic function of $[I]$.

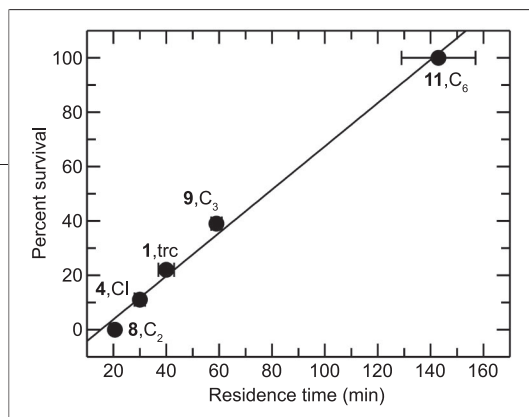


Figure 6. Linear correlation between percent survival and residence time. A linear fit to the data from Table 2 for compound residence time and percent survival in an animal model of infection gave a straight line with $r = 0.99$.

11 is more active in the animal model of infection than triclosan. Indeed, a positive linear correlation can be observed between the residence time of each compound on the enzyme and the *in vivo* antibacterial activity as gauged by the number of animals that survived to day 10 (Figure 6). This strongly suggests that the enhanced *in vivo* antibacterial activity of **11** is a direct consequence of the longer residence time of this compound on the enzyme drug target.

Slow-Onset Inhibitors and Drug Discovery. Recently Swinney (31) provided a perspective on the importance of slow, tight-binding inhibitors as drug candidates and pointed out that the efficiency and potency of classical competitive inhibitors, which establish rapid equilibrium binding with the target, would be greatly diminished with the accumulation of substrates in the open system. In order to avoid this and maintain *in vivo* efficiency, non-equilibrium-based inhibitors such as those that operate through a two-step slow-onset mechanism (Scheme 1, panel c) should be emphasized in drug discovery programs. A slow-onset inhibitor with a long drug target residence time can effectively create a transition away from rapid equilibrium inhibition and prevent the equilibrium between inhibitor and substrate from being achieved. Recent studies support the notion that longer residence time can improve target selectivity and reduce the side effects of small molecule inhibitors (19). In this context, Schramm and colleagues (32) have noted that DADMe-ImmH, a slow-onset inhibitor of purine nucleoside phosphorylase (PNP), is the ultimate

physiological inhibitor because it remains bound to PNP for the lifetime of the target in the cell.

Conclusion. The most potent diphenyl ether based compounds in the present study are slow-onset inhibitors of *fts* FabI. On the basis of a series of studies with this and other FabI enzymes, we believe that the slow step in formation of the final enzyme–inhibitor complex involves ordering of the substrate binding loop (11, 26, 33, 34). To better understand the biochemical mechanism of these slow, tight-binding inhibitors and their relationship with *in vivo* efficacy, we used progress curve analysis to determine the pre-steady-state constants for the interaction of triclosan and selected diphenyl ethers with *fts* FabI. We show that the kinetics of enzyme inhibition and the residence time of the compounds on the enzyme is a better predictor for *in vivo* antibacterial activity and that the longer residence time of **11** on the enzyme might provide the molecular explanation for the increase of the *in vivo* efficacy of this compound compared with that of the other diphenyl ethers (19). Note that the *in vitro* MIC values for the other selected compounds are significantly better than **11**, yet **11**, which has the longest residence time on the enzyme, is the most potent compound *in vivo* (Figure 6). Although we are aware that many factors may contribute to differences in the *in vivo* activity of structurally related drugs and that even minor changes in structure can impact properties such as pharmacokinetics, the change in residence time observed between the five compounds evaluated here may have a critical impact on target selectivity and intracellular activity. The data highlight the issues in translating *in vitro* antibacterial activities, determined at constant drug concentrations, to *in vivo* systems where the drug concentration will fluctuate between doses. These studies have broad implications for drug discovery programs that are largely driven by the measurement of inhibitor activity under equilibrium conditions and show the benefit of determining both the kinetic and thermodynamics for the formation of drug–target complexes.

METHODS

Compound Synthesis. The compounds were available from previous work (25, 26, 35).

Determination of Enzyme Inhibition Constants. The *F. tularensis* FabI (*fts* FabI; FTT 0782) and crotonyl-CoA (Cr-CoA) were prepared as described in the Supporting Information and in ref 46, respectively. All kinetic experiments were carried out on a Cary

300 Bio (Varian) spectrophotometer at 25 °C in 30 mM PIPES, 150 mM NaCl, and 1.0 mM EDTA, pH 8.0 buffer. Kinetic parameters were determined spectrophotometrically by following the oxidation of NADH to NAD⁺ at 340 nm ($\epsilon = 6300 \text{ M}^{-1} \text{ cm}^{-1}$). Since most of the diphenyl ethers are slow-onset inhibitors and in each case bind preferentially to the E-NAD⁺ form of the enzyme (Scheme 1), typical progress curve analysis cannot be

used to obtain the inhibition constant since the concentration of NAD⁺ varies during the assay. Instead, ftuFabI (10 nM) was preincubated with a fixed concentration of NAD⁺, inhibitor (0–1000 μM), and DMSO (1%, v/v) in the presence of 250 μM NADH for 5 h at 4 °C. The mixture was then warmed to RT, and the reactions were initiated by the addition of Cr-CoA (160 μM). Equation 1 was used to estimate the apparent inhibition constant K_i' :

$$v = \frac{v_0}{1 + [I]/K_i'} \quad (1)$$

where v_0 is the rate in the absence of inhibitor and $[I]$ is the tris-closan concentration.

This experiment was repeated at varying concentrations of NAD⁺ (10–200 μM) and the mechanism of inhibition with respect to NAD⁺ was determined by fitting the data to eqs 2–4. K_1 and K_2 are defined in panels a and b in Scheme 1 and represent the equilibrium constants for inhibitor binding to E-NAD⁺ and E-NADH, respectively.

Inhibitor binds exclusively to the E-NAD⁺ form:

$$K_i' = \frac{K_1([NAD^+] + K_{m,NAD})}{[NAD^+]} \quad (2)$$

Inhibitor binds exclusively to the E-NADH form:

$$K_i' = \frac{K_2([NAD^+] + K_{m,NAD})}{K_{m,NAD}} \quad (3)$$

Inhibitor binds both to the E-NAD⁺ and E-NADH forms:

$$K_i' = K_2 \frac{1 + [NAD^+]/K_{m,NAD}}{1 + [NAD^+]/(K_{m,NAD}K_1/K_2)} \quad (4)$$

where the $K_{m,NAD}$ value for NAD⁺ was calculated from

$$K_{m,NAD} = K_{i,NAD}(1 + [NADH]/K_{m,NADH}) \quad (5)$$

and $K_{i,NAD}$ is the dissociation constant of NAD⁺. Equation 5 presumes that NAD⁺ is a competitive inhibitor with respect to NADH as was shown by the product inhibition studies (data not shown).

For those diphenyl ethers that were rapid reversible inhibitors, the concentration of inhibitor in each assay was at least 10-fold larger than the enzyme concentration, allowing the inhibition constants to be determined using standard Michaelis–Menten kinetics. Initial velocities were measured using a fixed Cr-CoA concentration (160 μM) and by varying the concentration of NADH and inhibitors. All these inhibitors were shown to be competitive with respect to NADH, and inhibition constants (K_{is}) were calculated by fitting the data to

$$v = \frac{V_{max}[S]}{K_m(1 + [I]/K_{is}) + [S]} \quad (6)$$

where $[S]$ is the concentration of NADH, K_m is the Michaelis–Menten constant for NADH, V_{max} is the maximum velocity, $[I]$ is the concentration of inhibitor added, and K_{is} is the inhibition constant.

X-ray Crystallography. For the crystallization of the ftuFabI-NAD⁺ complex, equal amounts of protein (5 mg mL^{−1} ftuFabI in 30 mM PIPES pH 8.0, 150 mM NaCl, and 1 mM EDTA) and precipitant solution (20% PEG 3350, 0.2 M Mg acetate, 2 mM NAD⁺) were mixed and equilibrated against the precipitant solution without NAD⁺. Crystals grew within 2 days and were transferred into precipitant solution containing 25% (v/v) glycerol and frozen in liquid nitrogen. Diffraction data were collected at beam line X26C at the National Synchrotron Light Source at Brookhaven National Laboratory and indexed, integrated, and scaled with HKL2000 (data collection statistics in Supplementary Table S1). The structure was solved by molecular replacement with the program Phaser (36), using one monomer of the apo form of the *F. tularensis* enoyl reductase (unpublished data) as the search model. Molecular replacement yielded four molecules in the crystallographic asymmetric unit that form a homotetramer. Only one NAD⁺ molecule was identified in the $F_o - F_c$ difference density map and was built into the electron density using Coot (37). Model building and refinement was carried out using alternating rounds of Coot for manual model building and Refmac (38) for maximum likelihood refinement. Four-fold non-crystallographic symmetry (NCS) restraints were maintained throughout refinement. Five percent of all reflections were omitted throughout the refinement for the calculation of R_{free} (refinement statistics in Supplementary Table S1).

Progress Curve Analysis. Progress curves were used to further quantitate the inhibition of ftuFabI by those compounds that were slow-onset inhibitors. In order to take into account the change in NAD⁺ concentration during the assay as mentioned above, assays contained 200 μM NAD⁺ in addition to ftuFabI (10 nM), Cr-CoA (160 μM), NADH (250 μM), inhibitor, and DMSO (1%, v/v). Reactions were allowed to proceed until the progress curve became linear, indicating that the steady-state velocity had been reached. Low enzyme concentrations were used to ensure only a small fraction of Cr-CoA and NADH was consumed during the course of measurement so that the progress curves were essentially linear in the absence of inhibitor. The resulting progress curves were fitted to the integrated rate equation

$$A_t = [A_0 - V_s t - (v_i - v_s)(1 - \gamma) \ln \{ [1 - \gamma \exp(-k_{obs} t)] / (1 - \gamma) \}] / k_{obs} \gamma \quad (7)$$

where $\gamma = [E](1 - v_s/v_i)^2/[I]$, v_i and v_s are the initial velocity and steady-state velocity, and k_{obs} is the observed rate constant. Values for v_i , v_s , and k_{obs} were extracted by fitting the data to eq 7 at each inhibitor concentration. Subsequently, K_i^{app} was calculated by fitting the values for k_{obs} to the equation for a two-step inhibition mechanism (eq 8) in which the initial rapid binding of the inhibitor to the enzyme is followed by a second slow step resulting in the final enzyme–inhibitor complex (Scheme 1, panel c).

$$k_{obs} = k_{-2} + \frac{k_2[I]}{K_i^{app} + [I]} \quad (8)$$

where $K_i^{app} = k_{-1}/k_1$.

In Vitro and in Vivo Antibacterial Activity. *F. tularensis* LVS was cultured in modified Mueller-Hinton broth medium (0.025% ferric pyrophosphate, 2% IsoVitalEx, and 0.1% glucose) or on modified Mueller-Hinton agar medium (0.025% ferric pyrophosphate, 2% IsoVitalEx, 0.1% glucose, and 0.025% FBS) as previously described (39). MIC values were determined via NCCLS protocols using modified Mueller-Hinton broth as previously described (40). Compounds were tested at 2-fold serial concentrations from 0.000015 to 128 μg mL^{−1} in triplicate. MIC values

were determined by visual inspection after ~20 h at 37 °C and by Microplate Alamar blue assay (MABA) as described by Franzblau *et al.* (41) with modifications for *Francisella*.

Six-week-old female ICR mice were purchased from Charles River Laboratories. All mice were housed in sterile microisolate cages in the Laboratory Animal Resources facility or in the Biohazard Research Building BSL-3 facility at Colorado State University. All research involving animals was conducted in accordance with animal care and use guidelines, and animal protocols were approved by the Animal Care and Use Committee at Colorado State University. Mice were infected with *F. tularensis* Schu4 via low-dose aerosol infections in a Glascol Inhalation Exposure System (Glas-Col, Inc., Terre Haute, IN). Prior to exposure, the nebulizer was loaded with bacteria diluted in PBS to a concentration of approximately 5×10^6 cfu mL⁻¹. Mice were exposed to a total of approximately 4×10^7 bacteria aerosolized into a volume of 5 cubic feet over a period of 30 min, followed by a 20 min period of cloud decay when airflow was maintained but bacteria were no longer introduced. Drugs were formulated in 5% ethanol–water with the exception of triclosan, which was formulated in 8% Solutol (BASF) and 5% ethanol–water. Either compound or vehicle as control were delivered intraperitoneally once per day for 5 days at 200 mg kg⁻¹ day⁻¹ beginning at the time of challenge. Mice were monitored for morbidity and mortality twice daily for a period of 10 days, at which time survivors were euthanized. Efficacy was determined from median survival values and percent survival to day 10.

Cytotoxicity Evaluation. African green monkey kidney cells (Vero cells) were grown in RPMI 1640 medium supplemented with 1.5 g L⁻¹ sodium bicarbonate, 10 mL L⁻¹ 100 mM sodium pyruvate, 140 mL L⁻¹ 100x nonessential amino acids, 100 mL L⁻¹ penicillin-streptomycin solution (10,000 IU/10,000 µg mL⁻¹), and 10% bovine calf serum at 37 °C in a 5% CO₂ incubator with 75% humidity. Compounds were evaluated at 2-fold serial concentrations from 0.000015 to 128.0 µg mL⁻¹ in triplicate. Following compound addition, cells were incubated for 72 h at 37 °C in a 5% CO₂ incubator. The cells were then washed with PBS, CellTiter 96 AQueous One solution was added to each well, and plates were incubated for 4 h at 37 °C. Plates were read at 490 nm using a spectrophotometric plate reader, and the absorbance readings were used to calculate the 50% lethal concentration (LC₅₀) using GraFit software as previously described (42).

Acknowledgment: This work was supported by New Opportunities funding to P.J.T. and R.A.S. from the Northeast Biodefense Center (AI057158) and the Rocky Mountain Regional Center of Excellence (AI065357), as well as National Institutes of Health grants AI44639 and AI70383 to P.J.T.

Supporting Information Available: This material is available free of charge via the Internet at <http://pubs.acs.org>.

REFERENCES

- Sjostedt, A. (2006) Intracellular survival mechanisms of *Francisella tularensis*, a stealth pathogen, *Microbes Infect.* 8, 561–567.
- Oyston, P. C., Sjostedt, A., and Titball, R. W. (2004) Tularemia: bioterrorism defence renews interest in *Francisella tularensis*, *Nat. Rev. Microbiol.* 2, 967–978.
- White, S. W., Zheng, J., Zhang, Y. M., and Rock, C. O. (2005) The structural biology of type II fatty acid biosynthesis, *Annu. Rev. Biochem.* 74, 791–831.
- Bergler, H., Fuchsichler, S., Hogenauer, G., and Tumowsky, F. (1996) The enoyl-[acyl-carrier-protein] reductase (FabI) of *Escherichia coli*, which catalyzes a key regulatory step in fatty acid biosynthesis, accepts NADH and NADPH as cofactors and is inhibited by palmitoyl-CoA, *Eur. J. Biochem.* 242, 689–694.
- Zhang, Y. M., White, S. W., and Rock, C. O. (2006) Inhibiting bacterial fatty acid synthesis, *J. Biol. Chem.* 281, 17541–17544.
- Heath, R. J., and Rock, C. O. (2004) Fatty acid biosynthesis as a target for novel antibacterials, *Curr. Opin. Invest. Drugs* 5, 146–153.
- Campbell, J. W., and Cronan, J. E., Jr. (2001) Bacterial fatty acid biosynthesis: targets for antibacterial drug discovery, *Annu. Rev. Microbiol.* 55, 305–332.
- Payne, D. J., Warren, P. V., Holmes, D. J., Ji, Y., and Lonsdale, J. T. (2001) Bacterial fatty-acid biosynthesis: a genomics-driven target for antibacterial drug discovery, *Drug Discovery Today* 6, 537–544.
- Seefeld, M. A., Miller, W. H., Newlander, K. A., Burgess, W. J., DeWolf, W. E., Jr., Elkins, P. A., Head, M. S., Jakas, D. R., Janson, C. A., Keller, P. M., Manley, P. J., Moore, T. D., Payne, D. J., Pearson, S., Polizzi, B. J., Qiu, X., Rittenhouse, S. F., Uzinskas, I. N., Wallis, N. G., and Huffman, W. F. (2003) Indole naphthyridinones as inhibitors of bacterial enoyl-ACP reductases FabI and FabK, *J. Med. Chem.* 46, 1627–1635.
- Karlowsky, J. A., Laing, N. M., Baudry, T., Kaplan, N., Vaughan, D., Hoban, D. J., and Zhanel, G. G. (2007) In vitro activity of API-1252, a novel FabI inhibitor, against clinical isolates of *Staphylococcus aureus* and *Staphylococcus epidermidis*, *Antimicrob. Agents Chemother.* 51, 1580–1581.
- Lu, H., and Tonge, P. J. (2008) Inhibitors of FabI, an enzyme drug target in the bacterial fatty acid biosynthesis pathway, *Acc. Chem. Res.* 41, 11–20.
- Moir, D. T. (2005) Identification of inhibitors of bacterial enoyl-acyl carrier protein reductase, *Curr. Drug Targets Infect. Disord.* 5, 297–305.
- Heath, R. J., Li, J., Roland, G. E., and Rock, C. O. (2000) Inhibition of the *Staphylococcus aureus* NADPH-dependent enoyl-acyl carrier protein reductase by triclosan and hexachlorophene, *J. Biol. Chem.* 275, 4654–4659.
- McMurry, L. M., McDermott, P. F., and Levy, S. B. (1999) Genetic evidence that InhA of *Mycobacterium smegmatis* is a target for triclosan, *Antimicrob. Agents Chemother.* 43, 711–713.
- McMurry, L. M., Oethinger, M., and Levy, S. B. (1998) Triclosan targets lipid synthesis, *Nature* 394, 531–532.
- Parikh, S. L., Xiao, G., and Tonge, P. J. (2000) Inhibition of InhA, the enoyl reductase from *Mycobacterium tuberculosis*, by triclosan and isoniazid, *Biochemistry* 39, 7645–7650.
- Stewart, M. J., Parikh, S., Xiao, G., Tonge, P. J., and Kisker, C. (1999) Structural basis and mechanism of enoyl reductase inhibition by triclosan, *J. Mol. Biol.* 290, 859–865.
- Ward, W. H., Holdgate, G. A., Rowsell, S., McLean, E. G., Pauptit, R. A., Clayton, E., Nichols, W. W., Colls, J. G., Minshull, C. A., Jude, D. A., Mistry, A., Timms, D., Camble, R., Hales, N. J., Britton, C. J., and Taylor, I. W. (1999) Kinetic and structural characteristics of the inhibition of enoyl (acyl carrier protein) reductase by triclosan, *Biochemistry* 38, 12514–12525.
- Copeland, R. A., Pompliano, D. L., and Meek, T. D. (2006) Drug-target residence time and its implications for lead optimization, *Nat. Rev. Drug Discovery* 5, 730–739.
- Tummino, P. J., and Copeland, R. A. (2008) Residence time of receptor-ligand complexes and its effect on biological function, *Biochemistry* 47, 8465.
- Sivaraman, S., Zwahlen, J., Bell, A. F., Hedstrom, L., and Tonge, P. J. (2003) Structure-activity studies of the inhibition of FabI, the enoyl reductase from *Escherichia coli*, by triclosan: kinetic analysis of mutant FabIs, *Biochemistry* 42, 4406–4413.
- Levy, C. W., Roujeinikova, A., Sedelnikova, S., Baker, P. J., Stuitje, A. R., Slabas, A. R., Rice, D. W., and Rafferty, J. B. (1999) Molecular basis of triclosan activity, *Nature* 398, 383–384.

23. Kuo, M. R., Morbidoni, H. R., Alland, D., Sneddon, S. F., Gourlie, B. B., Staveski, M. M., Leonard, M., Gregory, J. S., Janjigian, A. D., Yee, C., Musser, J. M., Kreiswirth, B., Iwamoto, H., Perozzo, R., Jacobs, W. R., Jr., Sacchettini, J. C., and Fidock, D. A. (2003) Targeting tuberculosis and malaria through inhibition of enoyl reductase: compound activity and structural data, *J. Biol. Chem.* **278**, 20851–20859.
24. Perozzo, R., Kuo, M., Sidhu, A. S., Valiyaveetil, J. T., Bittman, R., Jacobs, W. R., Jr., Fidock, D. A., and Sacchettini, J. C. (2002) Structural elucidation of the specificity of the antibacterial agent triclosan for malarial enoyl acyl carrier protein reductase, *J. Biol. Chem.* **277**, 13106–13114.
25. Sivaraman, S., Sullivan, T. J., Johnson, F., Novichenok, P., Cui, G., Simmerling, C., and Tonge, P. J. (2004) Inhibition of the bacterial enoyl reductase FabI by triclosan: a structure-reactivity analysis of FabI inhibition by triclosan analogues, *J. Med. Chem.* **47**, 509–518.
26. Sullivan, T. J., Truglio, J. J., Boyne, M. E., Novichenok, P., Zhang, X., Stratton, C. F., Li, H. J., Kaur, T., Amin, A., Johnson, F., Slayden, R. A., Kisker, C., and Tonge, P. J. (2006) High affinity InhA inhibitors with activity against drug-resistant strains of *Mycobacterium tuberculosis*, *ACS Chem. Biol.* **1**, 43–53.
27. Baldock, C., Rafferty, J. B., Sedelnikova, S. E., Baker, P. J., Stuitje, A. R., Slabas, A. R., Hawkes, T. R., and Rice, D. W. (1996) A mechanism of drug action revealed by structural studies of enoyl reductase, *Science* **274**, 2107–2110.
28. Rafi, S. B., Cui, G., Song, K., Cheng, X., Tonge, P. J., and Simmerling, C. (2006) Insight through molecular mechanics Poisson-Boltzmann surface area calculations into the binding affinity of triclosan and three analogues for FabI, the *E. coli* enoyl reductase, *J. Med. Chem.* **49**, 4574–4580.
29. Morrison, J. F., and Walsh, C. T. (1988) The behavior and significance of slow-binding enzyme inhibitors, *Adv. Enzymol. Relat. Areas Mol. Biol.* **61**, 201–301.
30. Copeland, R. A. (2005) *Evaluation of Enzyme Inhibitors in Drug Discovery: A Guide for Medicinal Chemists and Pharmacologists (Methods of Biochemical Analysis)*, Wiley, Hoboken, NJ.
31. Swinney, D. C. (2004) Biochemical mechanisms of drug action: what does it take for success? *Nat. Rev. Drug Discovery* **3**, 801–808.
32. Lewandowicz, A., Tyler, P. C., Evans, G. B., Furneaux, R. H., and Schramm, V. L. (2003) Achieving the ultimate physiological goal in transition state analogue inhibitors for purine nucleoside phosphorylase, *J. Biol. Chem.* **278**, 31465–31468.
33. Tonge, P. J., Kisker, C., and Slayden, R. A. (2007) Development of modern InhA inhibitors to combat drug resistant strains of *Mycobacterium tuberculosis*, *Curr. Top. Med. Chem.* **7**, 489–498.
34. Xu, H., Sullivan, T. J., Sekiguchi, J., Kirikae, T., Ojima, I., Stratton, C. F., Mao, W., Rock, F. L., Alley, M. R., Johnson, F., Walker, S. G., and Tonge, P. J. (2008) Mechanism and inhibition of saFabI, the enoyl reductase from *Staphylococcus aureus*, *Biochemistry* **47**, 4228–4236.
35. am Ende, C. W., Knudson, S. E., Liu, N., Childs, J., Sullivan, T. J., Boyne, M., Xu, H., Gegina, Y., Knudson, D. L., Johnson, F., Peloquin, C. A., Slayden, R. A., and Tonge, P. J. (2008) Synthesis and *in vitro* anti-mycobacterial activity of B-ring modified diaryl ether InhA inhibitors, *Bioorg. Med. Chem. Lett.* **18**, 3029–3033.
36. McCoy, A. J., Grosse-Kunstleve, R. W., Adams, P. D., Winn, M. D., Storoni, L. C., and Read, R. J. (2007) Phaser crystallographic software, *J. Appl. Crystallogr.* **40**, 658–674.
37. Emsley, P., and Cowtan, K. (2004) Coot: model-building tools for molecular graphics, *Acta Crystallogr. D Biol. Crystallogr.* **60**, 2126–2132.
38. Winn, M. D., Isupov, M. N., and Murshudov, G. N. (2001) Use of TLS parameters to model anisotropic displacements in macromolecular refinement, *Acta Crystallogr. D Biol. Crystallogr.* **57**, 122–133.
39. Bosio, C. M., and Dow, S. W. (2005) *Francisella tularensis* induces aberrant activation of pulmonary dendritic cells, *J. Immunol.* **175**, 6792–6801.
40. Baker, C. N., Hollis, D. G., and Thornsberry, C. (1985) Antimicrobial susceptibility testing of *Francisella tularensis* with a modified Mueller-Hinton broth, *J. Clin. Microbiol.* **22**, 212–215.
41. Franzblau, S. G., Witzig, R. S., McLaughlin, J. C., Torres, P., Madico, G., Hernandez, A., Degnan, M. T., Cook, M. B., Quenzer, V. K., Ferguson, R. M., and Gilman, R. H. (1998) Rapid, low-technology MIC determination with clinical *Mycobacterium tuberculosis* isolates by using the microplate Alamar Blue assay, *J. Clin. Microbiol.* **36**, 362–366.
42. Boyne, M. E., Sullivan, T. J., am Ende, C. W., Lu, H., Gruppo, V., Heaslip, D., Amin, A. G., Chatterjee, D., Lenaerts, A., Tonge, P. J., and Slayden, R. A. (2007) Targeting fatty acid biosynthesis for the development of novel chemotherapeutics against *Mycobacterium tuberculosis*: evaluation of A-ring-modified diphenyl ethers as high-affinity InhA inhibitors, *Antimicrob. Agents Chemother.* **51**, 3562–3567.
43. Krissinel, E., and Henrick, K. (2004) Secondary-structure matching (SSM), a new tool for fast protein structure alignment in three dimensions, *Acta Crystallogr. D Biol. Crystallogr.* **60**, 2256–2268.
44. Bailey, S. (1994) The Ccp4 Suite—programs for protein crystallography, *Acta Crystallogr. Sect. D Biol. Crystallogr.* **D50** 760–763.
45. Delano, W. L. (2002) The PyMOL Molecular Graphics System; <http://www.pymol.org>.
46. Hofstein, H. A., Feng, Y., Anderson, V. E., and Tonge, P. J. (1999) Role of glutamate 144 and glutamate 164 in the catalytic mechanism of enoyl-CoA hydratase, *Biochemistry* **38**, 9508–9516.